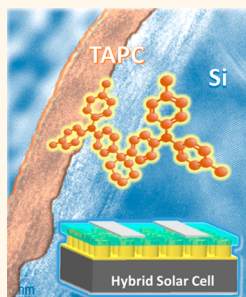


13% Efficiency Hybrid Organic/Silicon-Nanowire Heterojunction Solar Cell *via* Interface Engineering

Peichen Yu,^{†,*} Chia-Ying Tsai,[‡] Jan-Kai Chang,[§] Chih-Chung Lai,[⊥] Po-Han Chen,[†] Yi-Chun Lai,[†] Pei-Ting Tsai,[#] Ming-Chin Li,[‡] Huai-Te Pan,[†] Yang-Yue Huang,[†] Chih-I Wu,[§] Yu-Lun Chueh,[⊥] Shih-Wei Chen,^{||} Chen-Hsun Du,^{||} Sheng-Fu Horng,[‡] and Hsin-Fei Meng^{#,*}

[†]Department of Photonics and Institute of Electro-Optical Engineering, National Chiao-Tung University, Hsinchu 30010, Taiwan, [‡]Department of Electrical Engineering and Institute of Photonics Technologies, National Tsing-Hua University, Hsinchu 30071, Taiwan, [§]Department of Electrical Engineering and Graduate Institute of Photonics and Optoelectronics, National Taiwan University, Taipei 10617, Taiwan, [⊥]Department of Material Engineering, National Tsing-Hua University 30071, Hsinchu, Taiwan, ^{||}Green Energy and Environment Research Laboratories, Industrial Technology Research Institute, Hsinchu 31040, Taiwan, and [#]Institute of Physics, National Chiao-Tung University, Hsinchu 30010, Taiwan

ABSTRACT Interface carrier recombination currently hinders the performance of hybrid organic–silicon heterojunction solar cells for high-efficiency low-cost photovoltaics. Here, we introduce an intermediate 1,1-bis[(di-4-tolylamino)phenyl]cyclohexane (TAPC) layer into hybrid heterojunction solar cells based on silicon nanowires (SiNWs) and conjugate polymer poly(3,4-ethylenedioxy-thiophene):poly(styrenesulfonate) (PEDOT:PSS). The highest power conversion efficiency reaches a record 13.01%, which is largely ascribed to the modified organic surface morphology and suppressed saturation current that boost the open-circuit voltage and fill factor. We show that the insertion of TAPC increases the minority carrier lifetime because of an energy offset at the heterojunction interface. Furthermore, X-ray photoemission spectroscopy reveals that TAPC can effectively block the strong oxidation reaction occurring between PEDOT:PSS and silicon, which improves the device characteristics and assurances for reliability. These learnings point toward future directions for versatile interface engineering techniques for the attainment of highly efficient hybrid photovoltaics.



KEYWORDS: hybrid solar cell · interface engineering · conductive polymer · small molecule

As photovoltaics have garnered significant attention due to rising concerns with petroleum scarcity and global warming effects, its operation price is still not as competitive as others based on fossil fuels and hence not as widely deployed. Within current photovoltaic technologies, silicon-based solar cells dominate the market with over 80% share owing to high efficiency, reliability, and nontoxic earth-abundant resources.¹ The cost of silicon solar cells mainly arises from energy-intensive wafer purification and fabrication processes, which make for ~50 and ~25% of the total cost, respectively.² While the silicon photovoltaic industry is refining on several thin-wafer or thin-film technologies to reduce the material cost,³ there are very limited solutions to cut down the fabrication processes significantly. Recently, the emergence of hybrid organic–silicon solar cells offers a practical means to reduce cost by adopting low-temperature, scalable, and

soluble processes of conjugated polymers to form heterojunctions with silicon at the interface.^{4–12} By further adapting a thin film template, the hybrid heterojunction approach could make silicon-based solar cells a very viable option for next-generation photovoltaics.

Since the device structure of a hybrid organic–silicon solar cell is rather straightforward, normally composed of anode/p-type organic emitter/n-type silicon base/cathode, the power conversion efficiency (PCE) is fundamentally determined by optical absorption in the silicon absorber, charge transport associated with organic morphology and contact properties,¹³ as well as various carrier recombination mechanisms.^{14,15} Over the past few years, multiple studies have addressed these issues by using silicon textures for light harvesting,^{16–20} surfactant-treated conductive polymer for high conductivity,^{21–24} organic interface passivation,^{25–28} etc., leading to notable efficiency

* Address correspondence to yup@faculty.nctu.edu.tw, meng@mail.nctu.edu.tw.

Received for review July 31, 2013 and accepted November 13, 2013.

Published online November 13, 2013
10.1021/nn403982b

© 2013 American Chemical Society

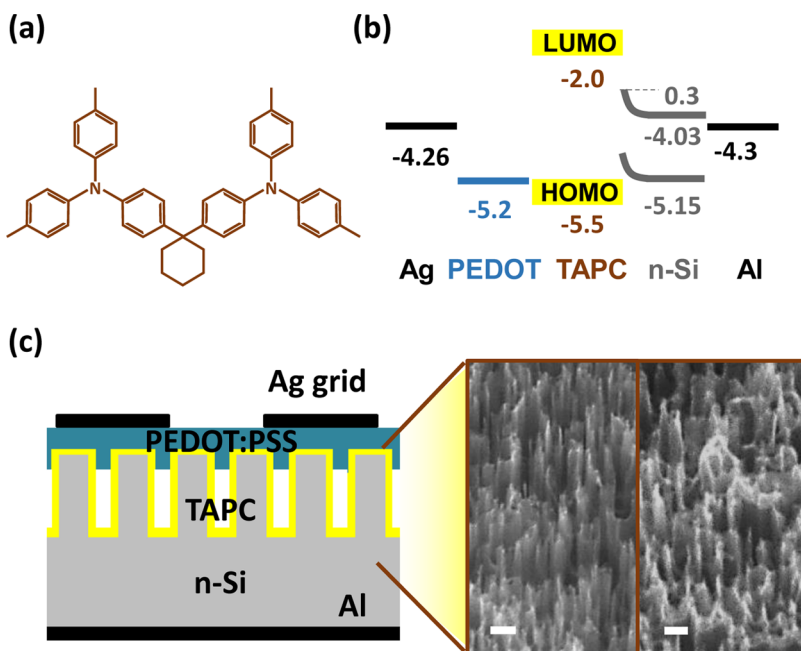


Figure 1. (a) Chemical structure of small-molecule TAPC. (b) Energy band diagram of a hybrid heterojunction solar cell based on silicon and PEDOT:PSS with an intermediate TAPC layer. (c) Fabricated device schematic with insets showing the structure of pristine silicon nanowires on the left and the morphology of spun-casted TAPC on the right.

improvements with PCEs ranging from 10 to 12%. According to these reports, it has been identified that the interface defect density plays a significant role in device characteristics. A theoretical model has also suggested that the fill factor and open-circuit voltage can be increased by another 15–20% if the defect density of states can be suppressed by 2 orders of magnitude, which is practical in conventional silicon solar cell technologies.¹⁹ To maintain the solution process advantages of hybrid heterojunction solar cells, herein we introduce an intermediate soluble 1,1-bis[(di-4-tolylamino)phenyl]cyclohexane (TAPC) layer at the organic–silicon interface of hybrid heterojunction solar cells based on silicon nanowires (SiNWs) and conjugate polymer poly(3,4-ethylenedioxythiophene):poly(styrenesulfonate) (PEDOT:PSS).²⁹ The combination of silicon nanostructures with the highly conductive conjugated polymer offer excellent light harvesting, charge transport, and collection capabilities, with the intermediate layer playing a significant role in mitigating the interface recombination. As a result, the highest PCE reaches a record 13.01% (average 12.54%), in comparison to 12.01% (average 11.55%) from the reference counterpart without TAPC. We further show that the TAPC layer improves the interface quality by serving three functions to boost the device performance. First, TAPC modifies the surface morphology of PEDOT:PSS laying atop SiNWs, which improves lateral carrier transport. Second, TAPC suppresses the saturation current *via* a large electron barrier at the interface, leading to an increased open circuit voltage. Finally, TAPC can effectively block the strong oxidation reaction occurring between PEDOT:

PSS and silicon, showing greater assurances for device reliability.

RESULTS AND DISCUSSION

TAPC is a soluble, small-molecule material (Figure 1a), which has been widely used in organic light emitting diodes as the hole transport layer because of a relatively high hole mobility of $\sim 10^{-2} \text{ cm}^2 \text{ V}^{-1} \text{ s}^{-1}$ at room temperature.^{30–32} Compared to other materials with high hole mobilities, TAPC possesses a small lowest-unoccupied-molecular-orbital (LUMO) value of 2.0 eV and a highest-occupied-molecular-orbital (HOMO) of 5.5 eV comparable to that of PEDOT:PSS.³³ Therefore, the insertion of TAPC into the organic/silicon interface of a hybrid solar cells results in an energy band diagram as shown in Figure 1b. Here, the amount of surface band bending and the ionization energy of TAPC on SiNWs have been experimentally determined by X-ray and UV photoelectron spectroscopy (XPS and UPS) (see Supporting Information). Since the energy offset with respect to the conduction band of silicon is as large as 2.03 eV, TAPC can also function as an electron blocking layer to suppress electron injection from the anode under reverse bias, leading to a reduced dark current in the device. The fabricated device schematic is illustrated in Figure 1c, where the insets compare the morphology of pristine SiNWs (left) and those with spun-casted TAPC (right). It can be observed that the small-molecule material is capable of reaching into the spacings of SiNWs, forming a conformal thin-film coating on the side walls. The scanning electron micrographs (SEMs) of the hybrid solar cells with and without the TAPC layer are also investigated in tilted top and

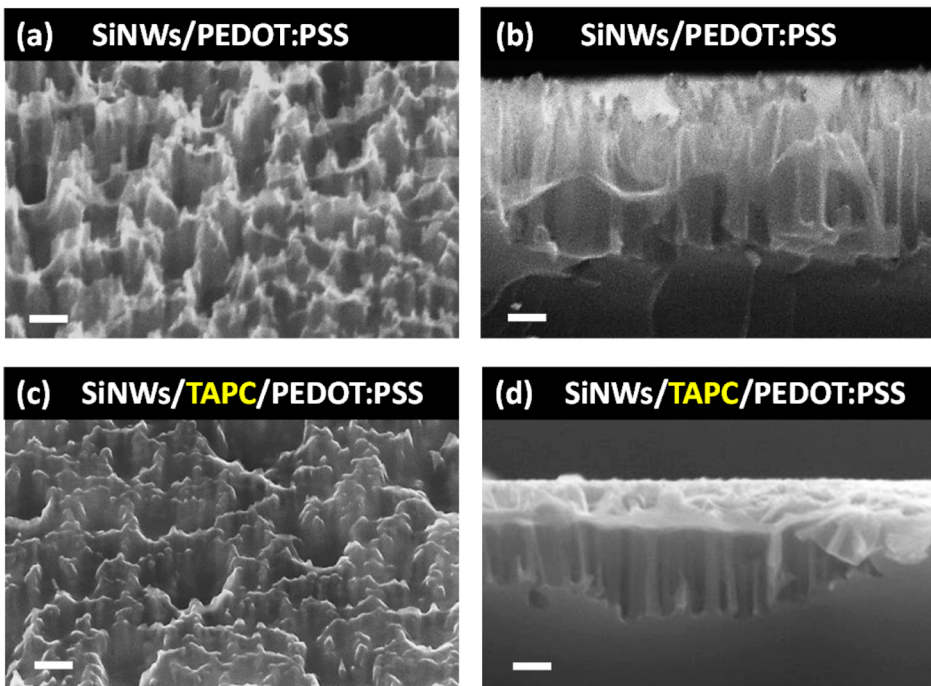


Figure 2. (a) Surface and (b) cross-sectional morphology of PEDOT:PSS coated on silicon nanowires (SiNWs). (c,d) Corresponding images for the device structure an intermediate TAPC layer. The scalar bar is 100 nm.

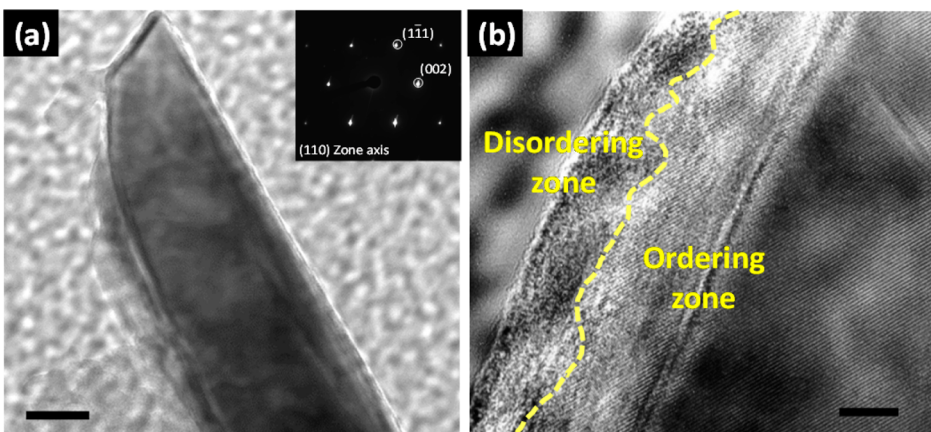


Figure 3. (a) High-resolution TEM image of individual Si/TAPC core–shell nanorod, which is confirmed by the single crystalline structure of a selective-area diffraction pattern as shown in the inset. The scalar bar represents 20 nm in length. (b) The interface of TAPC and Si is indicated by yellow dashed line for clarity, where TAPC is indicated by the amorphous region, approximately 6–8 nm in thickness. The scalar bar represents 5 nm in length.

cross-sectional views. As seen in Figure 2a, the spin-coated PEDOT:PSS layer on top of the nanowire cluster with a spin rate of 8000 rpm is quite thin and appears to sink halfway into the nanowire gap (Figure 2b). In this core–sheath junction configuration, lateral hole transport to the silver finger grid is likely impeded by surface recombination due to complex conducting routes. Moreover, it is difficult to examine the organic surface coverage on the tips of nanowires because of nanoscale dimensions. In contrast, as seen in Figure 2c, the surface morphology of PEDOT:PSS with a TAPC layer underneath appears to be thicker than that of the reference sample. The morphology at the tips of SiNWs is more rounded, instead of pointy, which assures the complete

PEDOT:PSS coverage on the nanotextured surface. It is also evident, from the side view, that a relatively planar PEDOT:PSS thin film lays on top of the nanowires, indicating a shorter charge transport route than the reference to lateral electrical contacts. By comparing Figure 2b to 2c, the heterojunction area and organic layer thickness of the solar cell without TAPC are larger and thinner than those with TAPC. Although a large junction area may be beneficial for charge separation and carrier collection, it is also accompanied by deteriorated surface recombination and increased sheet resistance due to the thin organic thickness. Moreover, incomplete organic surface coverage at the tips of nanowires may give rise to additional device

degradation.^{34–36} From these points of view, the morphology modification induced by TAPC is advantageous to the photovoltaic characteristics of hybrid solar cells.

To further understand the material property of the TAPC layer, the coating on the side wall of a single nanowire is examined by a high-resolution transmission electron microscope (HR-TEM). The sample is prepared by scraping the nanowires off the substrate after spin-casting with TAPC at a rate of 4000 rpm. Figure 3a shows the core–shell Si/TAPC structure of a single nanowire. The single crystalline structure of nanowires is confirmed by a selected-area-diffraction (SAD) pattern as shown in the inset. The interface of TAPC and Si is indicated by yellow dashed line for clarity. It has been reported that silicon nanowires fabricated by metal-assisted chemical etching (MACE) have rough side wall surfaces,^{37–39} which can be identified from the atomic ordering zone as seen in Figure 3b. Outside the ordering regime, the amorphous region shows the TAPC layer with a thickness of approximately 6–8 nm. Since the HOMO level of TAPC is slightly lower than that of PEDOT:PSS by 0.3 eV,³³ it is essential that the surface coating of TAPC onto the side wall of silicon nanowires be very thin in order to facilitate hole transport across the TAPC/PEDOT:PSS interface. The TEM images confirm that solution-processed TAPC fulfills the purpose as a thin intermediate layer.

Next, the current density–voltage (J – V) characteristics of the best-performing devices in light and dark conditions are respectively plotted in Figure 4a,b for samples with and without the intermediate TAPC layer, whereas the overall device statistics, including average and standard deviation for short-circuit current density (J_{sc}), V_{oc} , FF, and PCE are summarized in Table 1. As shown in Figure 4a, the best hybrid heterojunction cell demonstrates a record PCE of 13.01% with a high J_{sc} of 34.76 mA/cm², both of which are superior to the reference counterpart of 12.01% and 34.46 mA/cm². We note that the enhancement also results from an improved V_{oc} from 0.52 to 0.54 V, and a FF from 66.4 to 69.5%. The increase of V_{oc} from the device with the TAPC layer is justified by the reduced saturation current in the dark J – V curve by almost an order of magnitude lower than the reference counterpart. Since the source of dark reversed current is originated from thermionic emission of electrons and holes from the anode and cathode, the large electron barrier presented by TAPC at the PEDOT:PSS/silicon interface is useful to block electrons and hence reduce the saturation current. On the other hand, when the device is forward biased and under illumination, the energy offset of TAPC can also block electron injection from the cathode, leading to a reduced recombination loss at the interface and increasing the shunt resistance and FF. We reckon that the hole transport under dark and

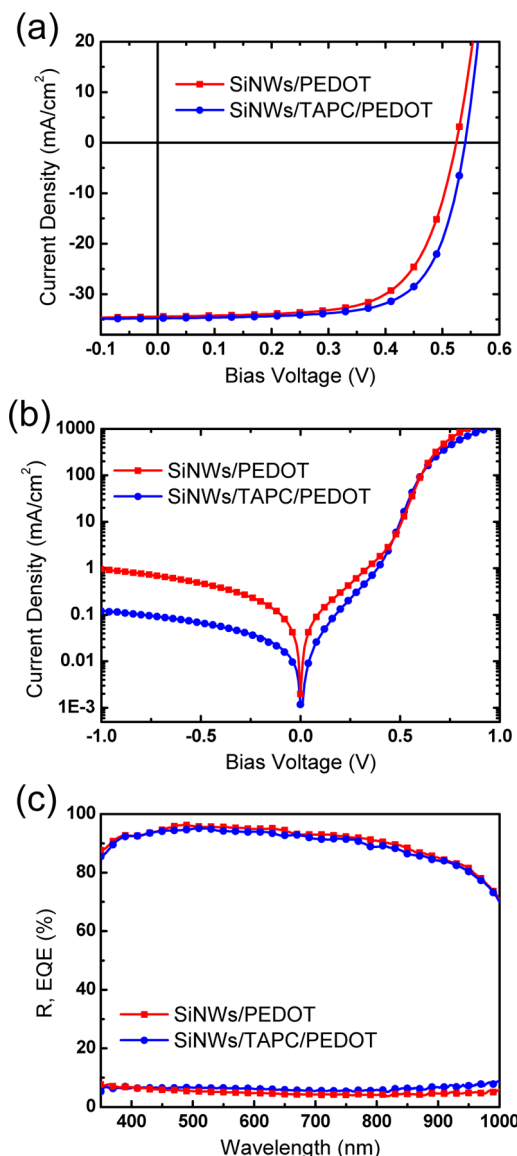


Figure 4. (a) Current density–voltage characteristics of the hybrid solar cells under a simulated AM1.5G illumination condition. (b) Dark current density–voltage characteristics in semilogarithm plot. (c) Reflectance (R), and external quantum efficiency (EQE) spectra of the fabricated devices with and without the TAPC layer.

TABLE 1. Photovoltaic Characteristics^a, Including Short-Circuit Current Density (J_{sc}), Open-Circuit Voltage (V_{oc}), Fill Factor (FF), and Power Conversion Efficiency (PCE) of Hybrid Heterojunction Solar Cells with and without the Intermediate TAPC Layer

devices	J_{sc} (mA/cm ²)	V_{oc} (V)	FF (%)	PCE (%)
w/o TAPC	34.34 ± 0.14	0.52 ± 0.005	64.15 ± 2.83	11.55 ± 0.50
w/TAPC	34.81 ± 0.05	0.54 ± 0.005	67.08 ± 2.27	12.54 ± 0.49

^a Values are obtained by averaging three devices with a calculated confidence interval of 95%.

illuminated conditions is not affected for this device with TAPC, as the hole barrier is small and the TAPC layer is very thin. This hypothesis is confirmed by the

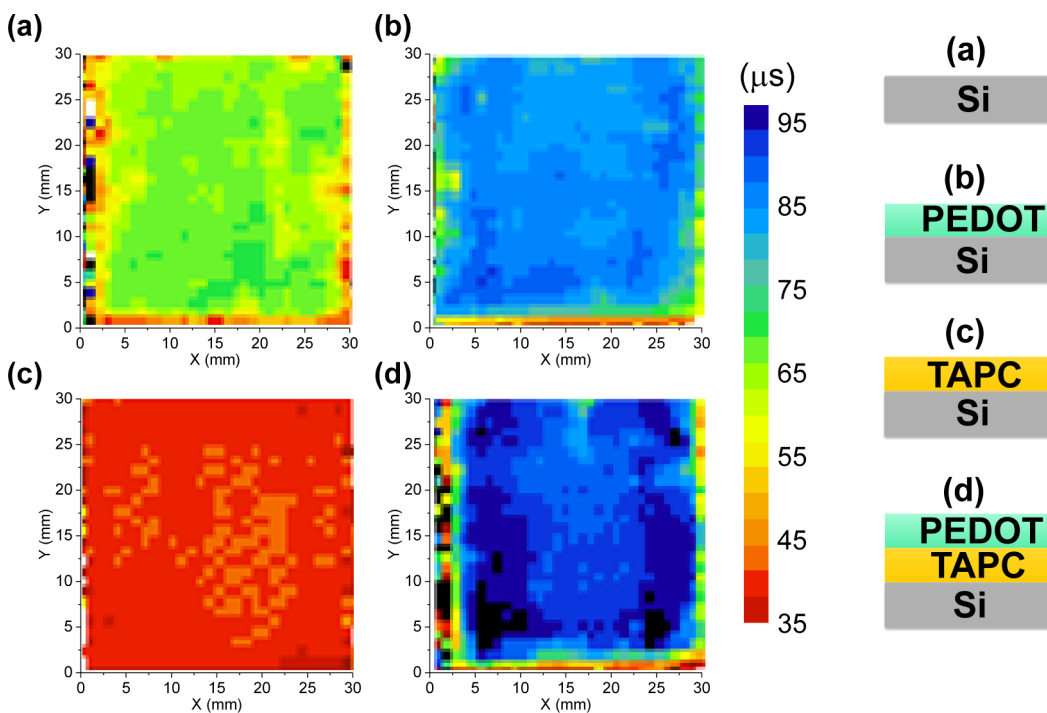


Figure 5. (a–d) Spatial mapping of the minority carrier lifetime from four different samples with corresponding structures schematically shown on the right. The planar silicon wafers are prepared with a $3 \times 3 \text{ cm}^2$ surface area.

similar light currents of the two devices, both reaching a high photocurrent level above 34 mA/cm^2 . Moreover, the reflectance (R) and external quantum efficiency (EQE) spectra (Figure 4c) also show nearly identical values for all wavelengths. Figure 4c further showcases the advantages of hybrid heterojunction device characteristics. First, the surface reflection of the device is extremely low with the SiNW template $\sim 7\text{--}8\%$ and shows nearly flat spectral responses due to its excellent light harvesting capability. Second, the EQE demonstrates very high efficiencies above 90% across the broad spectral range (375–825 nm), particularly in the blue wavelength regime, demonstrating low surface recombination in the heterojunction device architecture based on silicon and PEDOT:PSS.

To investigate the organic–silicon interface quality with TAPC, we conduct a spatial mapping of minority carrier lifetime measurement based on a microwave photoconductance decay (μ -PCD) technique (WT-2000PVN, Semilab). The minority carrier lifetime in a silicon solar cell depends on surface and bulk recombination and is dominated by the faster process,²⁶ as expressed in eq 1.

$$\frac{1}{\tau_{\text{meas}}} = \frac{1}{\tau_{\text{bulk}}} + \frac{2S}{w} \quad (1)$$

where τ_{meas} is the measured lifetime, τ_{bulk} is the bulk recombination lifetime, S is the surface recombination velocity, and w is the wafer thickness. Here we assume that both front and rear wafer surfaces have the same recombination velocities and neglected the time for carrier diffusion to the surface from the middle of the

wafer. Since the bulk lifetime of the silicon wafer is on the order of a few hundred microseconds to 1 ms, the measured lifetime of a silicon wafer without any surface passivation reflects the surface recombination rate. We first prepare four different samples in ambient conditions using the same n-type planar silicon wafer for devices and same cleaning procedures. The samples include (a) a planar silicon wafer as reference and three planar silicon wafers with (b) spun-casted PEDOT:PSS only, (c) spun-casted TAPC only, and (d) both TAPC and PEDOT:PSS on both sides of silicon. The lifetime mappings of the four samples are presented in Figure 5a–d, which correspond to an average lifetime of 66, 84, 39, and $88 \mu\text{s}$, respectively. As seen in Figure 5b, once the PEDOT:PSS and silicon form a heterojunction on the frontal surface, the minority carrier lifetime is increased from 66 to $84 \mu\text{s}$, as the built-in field swipes off carriers to prevent recombination at the interface. This observation is also supported by the high EQE in the short wavelength range. However, the silicon sample with TAPC suffers from severe surface recombination, where the average lifetime of $39 \mu\text{s}$ is much worse than that of the reference (Figure 5c). It is clear that TAPC does not have any passivation or junction formation effects on the silicon surface, and may act as the recombination center if present alone. However, the sample with both TAPC and PEDOT has the longest lifetime of $88 \mu\text{s}$ (Figure 5d), which is ascribed to heterojunction band offsets that mitigate interface recombination. Since the surface area of SiNWs is much larger than the planar wafer, we think that the interface band engineering is critical

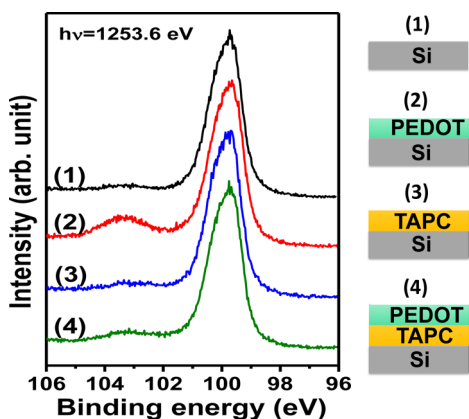


Figure 6. The X-ray photoemission spectra of silicon 2p core level from the silicon surface of four samples prepared in different surface conditions, as schematically shown on the right. The samples are exposed in ambient conditions for 12 h and then stripped off the organic TAPC and PEDOT materials prior to the measurement. The spectra were measured with a magnesium K α (1253.6 eV) photon line.

and effective to improve the V_{oc} and FF of hybrid heterojunction solar cells.

Besides carrier recombination, oxidation reaction at the organic–silicon interface is also of great interest and often depicts the device performance. The aforementioned four planar samples are prepared again and exposed in ambient conditions for 12 h to examine the oxidized interface by the XPS measurement. Therefore, prior to the measurement, the samples are cleaned with acetone, isopropyl alcohol (IPA), and deionized (DI) water in order to strip off the organic materials and uncover the silicon surface. The samples are then immediately loaded into the vacuum chamber for spectroscopy analysis, where the binding energies of core-level electrons were measured by using a magnesium K α (1253 eV) photon line. Figure 6 shows the

photoemission spectra from the silicon surface of the four samples. The binding energy of silicon 2p core level is around 100 eV,⁴⁰ which is the dominant peak in the spectra of Figure 6. It is observed that only the planar silicon sample with PEDOT:PSS shows an additional peak around 103 eV, which indicates the photoelectron emission from silicon dioxide (SiO₂). Additional XPS analyses are conducted for the surface of bare silicon exposed in ambient atmosphere for 4 days (Supporting Information Figure S3). It is revealed that the oxidation rate occurred at PEDOT:PSS/silicon interface for 12 h in ambient conditions is comparable to that of bare silicon exposed in air for 4 days. As clearly seen in Figure 6, the insertion of TAPC is capable of blocking the strong oxidation reaction occurring between PEDOT:PSS and silicon, which should be manifested in the SiNW template. Since the oxide layer impedes charge transport and often degrades the device performance if not well controlled, the insertion of an intermediate layer presents a viable approach to enhance the reliability of hybrid heterojunction solar cells.

CONCLUSION

In conclusion, interface engineering of hybrid heterojunction solar cells *via* an intermediate TAPC layer is demonstrated, which achieves a record power conversion efficiency of 13.01%. TAPC improves the morphology of PEDOT:PSS laying atop SiNWs, while a large electron barrier suppresses the interface recombination and dark saturation current, which leads to an enhanced open circuit voltage and fill factor. We further show that TAPC can effectively impede the strong oxidation reaction occurring at the PEDOT:PSS/silicon interface, hence facilitating charge transport in hybrid solar cells.

EXPERIMENTAL SECTION

Solar Cell Fabrication. The fabrication of hybrid heterojunction solar cells starts with preparing SiNW templates by using metal-assisted electrode-less chemical etching.⁴¹ First, n-type monocrystalline Si (100) substrates with a thickness of 650 μ m and a resistivity of 5 Ω ·cm were diced into tiles with areas of 3 \times 3 cm² and then immersed in a solution of hydrofluoric (HF) acid and silver nitride (AgNO₃) to etch the structure of nanowire arrays. The substrates were dipped in aqueous solution of nitric acid (HNO₃) and then rinsed with DI water, giving rise to vertically aligned nanowire clusters with lengths varying from 350 to 450 nm. The SiNW substrates were subsequently processed into hybrid solar cells. First, the samples were dipped in dilute hydrofluoric acid (DHF) for 15 s to remove the native oxide and attain a hydrophobic surface, followed by the thermal evaporation of a 100-nm-thick aluminum layer as the back electrode in the glovebox. 0.3 wt % TAPC was dissolved in chlorobenzene (CB) and then drop-cast onto the entire nanowire surface for 1 min to allow sufficient penetration into the spacings of nanowires before spin-coating at 4000 rpm for 100 s. A highly conductive aqueous PEDOT:PSS dispersion (Clevios PH1000) was employed with 5 wt % dimethyl sulfoxide (DMSO) as a secondary dopant to increase the conductivity.

Meanwhile, 0.3 wt % decaethylene glycol monododecyl ether (C₁₂E₁₀) surfactant was added to improve the uniformity of the PEDOT:PSS thin-film. The prepared PEDOT:PSS with additives was spun-cast onto the top of TAPC layer at a spin rate of 8000 rpm for 100 s and heated to 115 °C for 10 min in ambient conditions. Finally, a 100-nm-thick silver frontal electrode with a shading ratio of 16.67% was thermally evaporated through a shadow mask with four windows, each having an opening area of 0.5 \times 0.5 cm². A reference counterpart without the TAPC layer was also fabricated simultaneously.

Characterizations. A field emission scanning electron microscope (FE-SEM, JEOL JSM-7000F), operating at 10 kV, and a JEM-3000F field emission transmission electron microscope (FE-TEM) equipped with an energy dispersion spectrometer (EDS), operating at 300 kV, were used to study microstructures and surface morphologies. Reflectance spectra were measured by an UV–vis–NIR spectrophotometer (Hitachi U-4100). Photovoltaic characterizations of fabricated solar cells were performed under a simulated AM1.5G (Air Mass 1.5, Globe) illumination condition. The measurement system includes a power supply (Newport 69920), a 1000 W Class A solar simulator (Newport 91192A) with a Xenon lamp and an AM1.5G filter, a probe stage, and a source-meter (Keithley 2400) using a 4-wire connection

mode. The spectrum of the solar simulator was calibrated by a PV-measurement (PVM-154) monocrystalline Si solar cell (NREL calibrated), and a Si photo diode with KG-5 color filter (Hamamatsu, Inc.) was used to check the irradiation of the exposed area (100 mW/cm^2). The cell under test was shielded by a black stainless metal mask with an opening area of $0.3 \times 0.3 \text{ cm}^2$, and the temperature was actively controlled at $25 \pm 0.5^\circ\text{C}$ during the measurements.⁴²

The external quantum efficiency (EQE) system consists of a 450 W xenon lamp (Oriel Instrument, model 6266) light source, a water-based IR filter (Oriel Instrument, model 6123 NS), and a monochromator (Oriel Instrument, model 74,100). The incident light was focused on to a $1 \text{ mm} \times 3 \text{ mm}$ spot size between finger electrodes. A calibrated silicon photodetector (Newport 818-UV) was used to calibrate the EQE system before measurements. A lock-in amplifier (Standard Research System, SR830) and an optical chopper controller (SR540) in the voltage mode were also equipped to lock the output signal, and the photocurrent was converted to voltage using a 1 ohm resistor, which is in parallel with the sample. The cell's temperature was also actively controlled during the measurements at $25 \pm 0.5^\circ\text{C}$.⁴² X-ray photoemission experiments were carried out in an ultra-high vacuum chamber with a base pressure of 10^{-10} Torr. The energies of core-level electrons were measured by using a magnesium K α (1253.6 eV) photon line as the excitation source, where a double-pass cylindrical mirror analyzer is operated in retarding mode to measure energy spectra of photoelectrons.

Conflict of Interest: The authors declare no competing financial interest.

Acknowledgment. The authors thank the National Science Council in Taiwan for financial support under grant number 100-2628-E-009-020-MY3.

Supporting Information Available: Discussions about the relative energy positions and binding energy shifts of SiNWs/TAPC/PEDOT:PSS determined by X-ray and UV photoelectron spectroscopy. The X-ray photoemission spectra for various samples are also included to examine the oxidized interface. This information is available free of charge via the Internet at <http://pubs.acs.org/>.

REFERENCES AND NOTES

- Miles, R. W.; Zoppi, G.; Forbes, I. Inorganic Photovoltaic Cells. *Mater. Today* **2007**, *10*, 20–27.
- Fthenakis, V. M.; Kim, H. C. Photovoltaics: Life-Cycle Analyses. *Sol. Energy* **2011**, *85*, 1609–1628.
- Zweibel, K. Thin Film PV Manufacturing: Materials Costs and Their Optimization. *Sol. Energy Mater. Sol. Cells* **2000**, *63*, 375–386.
- Zhang, F.; Sun, B.; Song, T.; Zhu, X.; Lee, S. T. Air Stable, Efficient Hybrid Photovoltaic Devices Based on Poly(3-hexylthiophene) and Silicon Nanostructures. *Chem. Mater.* **2011**, *23*, 2084–2090.
- Zhang, F.; Han, X.; Lee, S. T.; Sun, B. Heterojunction with Organic Thin Layer for Three Dimensional High Performance Hybrid Solar Cells. *J. Mater. Chem.* **2012**, *22*, 5362–5368.
- Kalita, G.; Adhikari, S.; Aryal, H. R.; Afre, R.; Soga, T.; Sharon, M.; Koichi, W.; Umeno, M. Silicon Nanowire Array/Polymer Hybrid Solar Cell Incorporating Carbon Nanotubes. *J. Phys. D: Appl. Phys.* **2009**, *42*, 115104.
- Zhang, F.; Song, T.; Sun, B. Conjugated Polymer–Silicon Nanowire Array Hybrid Schottky Diode for Solar Cell Application. *Nanotechnology* **2012**, *23*, 194006.
- Shiu, S. C.; Chao, J. J.; Hung, S. C.; Yeh, C. L.; Lin, C. F. Morphology Dependence of Silicon Nanowire/Poly(3,4-ethylenedioxythiophene): Poly(styrenesulfonate) Heterojunction Solar Cells. *Chem. Mater.* **2010**, *22*, 3108–3113.
- Shen, X.; Sun, B.; Liu, D.; Lee, S. T. Hybrid Heterojunction Solar Cell Based on Organic–Inorganic Silicon Nanowire Array Architecture. *J. Am. Chem. Soc.* **2011**, *133*, 19408–19415.
- Ono, M.; Tang, Z.; Ishikawa, R.; Gotou, T.; Ueno, K.; Shirai, H. Efficient Crystalline Si/Poly(ethylene dioxythiophene): Poly(styrene sulfonate): Graphene Oxide Composite Heterojunction Solar Cells. *Appl. Phys. Express* **2012**, *5*, 032301.
- Zhu, Y.; Song, T.; Zhang, F.; Lee, S. T.; Sun, B. Efficient Organic–Inorganic Hybrid Schottky Solar Cell: The Role of Built-in Potential. *Appl. Phys. Lett.* **2013**, *102*, 113504.
- Xu, T.; Qiao, Q. Conjugated Polymer–Inorganic Semiconductor Hybrid Solar Cells. *Energy Environ. Sci.* **2011**, *4*, 2700.
- Price, M. J.; Foley, J. M.; May, R. A.; Maldonado, S. Comparison of Majority Carrier Charge Transfer Velocities at Si/Polymer and Si/Metal Photovoltaic Heterojunctions. *Appl. Phys. Lett.* **2010**, *97*, 083503.
- Tsai, S. H.; Chang, H. C.; Wang, H. H.; Chen, S. Y.; Lin, C. A.; Chen, S. A.; Chueh, Y. L.; He, J. H. Significant Efficiency Enhancement of Hybrid Solar Cells Using CoreShell Nanowire Geometry for Energy Harvesting. *ACS Nano* **2011**, *12*, 9501–9510.
- Zhang, J.; Zhang, Y.; Zhang, F.; Sun, B. Electrical Characterization of Inorganic–Organic Hybrid Photovoltaic Devices Based on Silicon–Poly(3,4-ethylenedioxythiophene): Poly(styrenesulfonate). *Appl. Phys. Lett.* **2013**, *102*, 013501.
- He, L.; Rusli; Jiang, C.; Wang, H.; Lai, D. Simple Approach of Fabricating High Efficiency Si Nanowire/Conductive Polymer Hybrid Solar Cells. *IEEE Electron Device Lett.* **2011**, *32*, 1406–1408.
- Jeong, S.; Garnett, E. C.; Wang, S.; Yu, Z.; Fan, S.; Brongersma, M. L.; McGehee, M. D.; Cui, Y. Hybrid Silicon Nanocone–Polymer Solar Cells. *Nano Lett.* **2012**, *12*, 2971–2976.
- He, L.; Jiang, C.; Rusli; Lai, D.; Wang, H. Highly Efficient Si-Nanorods/Organic Hybrid Core-Sheath Heterojunction Solar Cells. *Appl. Phys. Lett.* **2011**, *99*, 021104.
- Chen, T. G.; Huang, B. U.; Chen, E. C.; Yu, P.; Meng, H. F. Micro-Textured Conductive Polymer/Silicon Heterojunction Photovoltaic Devices with High Efficiency. *Appl. Phys. Lett.* **2012**, *101*, 033301.
- He, L.; Jiang, C.; Wang, H.; Lai, D.; Tan, Y. H.; Tan, C. S.; Rusli Effects of Nanowire Texturing on The performance of Si/Organic Hybrid Solar Cells Fabricated with a $2.2 \mu\text{m}$ Thin-Film Si Absorber. *Appl. Phys. Lett.* **2012**, *100*, 103104.
- He, L.; Jiang, C.; Wang, H.; Lai, D.; Rusli High Efficiency Planar Si/Organic Heterojunction Hybrid Solar Cells. *Appl. Phys. Lett.* **2012**, *100*, 073503.
- Liu, Q.; Ono, M.; Tang, Z.; Ishikawa, R.; Ueno, K. Highly Efficient Crystalline Silicon/Zonyl Fluorosurfactant-Treated Organic Heterojunction Solar Cells. *Appl. Phys. Lett.* **2012**, *100*, 183901.
- Alemu, D.; Wei, H. Y.; Ho, K. C.; Chu, C. Y. Highly Conductive PEDOT:PSS Electrode by Simple Film Treatment with Methanol for ITO-Free Polymer Solar Cells. *Energy Environ. Sci.* **2012**, *5*, 9662.
- Pietsch, M.; Bashouti, M. Y.; Christiansen, S. The Role of Hole Transport in Hybrid Inorganic/Organic Silicon/Poly(3,4-ethylenedioxythiophene):Poly(styrenesulfonate) Heterojunction Solar Cells. *J. Phys. Chem. C* **2013**, *117*, 9049–9055.
- Liu, D.; Zhang, Y.; Fang, X.; Zhang, F.; Song, T.; Sun, B. An 11%-Power-Conversion-Efficiency Organic–Inorganic Hybrid Solar Cell Achieved by Facile Organic Passivation. *IEEE Electron Device Lett.* **2013**, *34*, 345–347.
- Aberle, A. G. Surface Passivation of Crystalline Silicon Solar Cells: A Review. *Prog. Photovoltaics: Res. Appl.* **2000**, *8*, 473–487.
- Goh, C.; Scully, S. R.; McGehee, M. D. Effects of Molecular Interface Modification in Hybrid Organic–Inorganic Photovoltaic Cells. *J. Appl. Phys.* **2007**, *101*, 114503.
- Sushobhan Avasthi, S.; Qi, Y.; Vertelov, G. K.; Schwartz, J.; Kahn, A.; Sturm, J. C. Silicon Surface Passivation by An Organic Overlay of 9,10-phenanthrenequinone. *Appl. Phys. Lett.* **2010**, *96*, 222109.
- Tsai, C. Y.; Chen, P.-H.; Huang, Y.-Y.; Pan, H.-T.; Yu, P.; Meng, H. F. 11%-Efficiency Hybrid Organic/Silicon-Nanowire Heterojunction Solar Cell with an Intermediate 1,1-Bis[(di-4-tolylamino)phenyl]cyclohexane Layer. Presented at the

IEEE Photovoltaic Specialist Conference, Tampa, FL, June 16–21, **2013**.

- 30. Borsenberger, P. M.; Pautmeier, L.; Richert, R.; Bassler, H. Hole Transport in 1,1-Bis(di-4-tolylaminophenyl)cyclohexane. *Chem. Phys.* **1991**, *94*, 8276–8281.
- 31. Strohriegl, P.; Grazulevicius, J. V. Charge-Transporting Molecular Glasses. *Adv. Mater.* **2002**, *14*, 1439.
- 32. Yang, D.; Ma, D. 1,1-Bis[(di-4-tolylamino)phenyl]cyclohexane for Fast Response Organic Photodetectors with High External Efficiency and Low Leakage Current. *J. Mater. Chem. C* **2013**, *1*, 2054–2060.
- 33. Lin, L.-B.; Young, R. H.; Mason, M. G.; Jenekhe, S. A.; Borsenberger, P. M. Transient Photocurrents Across Organic–Organic Interfaces. *Appl. Phys. Lett.* **1998**, *72*, 864.
- 34. Song, T.; Lee, S. T.; Sun, B. Silicon Nanowires for Photovoltaic Applications: The Progress and Challenge. *Nano Energy* **2012**, *1*, 654–673.
- 35. Shiu, S. C.; Chao, J. J.; Hung, S. C.; Yeh, C. L.; Lin, C. F. Morphology Dependence of Silicon Nanowire/Poly(3,4-ethylenedioxythiophene): Poly(styrenesulfonate) Heterojunction Solar Cells. *Chem. Mater.* **2010**, *22*, 3108–3113.
- 36. Lu, W.; Wang, C.; Yue, W.; Chen, L. Si/PEDOT:PSS Core/Shell Nanowire Arrays for Efficient Hybrid Solar Cells. *Nanoscale* **2011**, *3*, 3631.
- 37. Rykaczewski, K.; Hildreth, O. J.; Wong, C. P.; Fedorov, A. G.; Scott, J. H. J. Guided Three Dimensional Catalyst Folding During Metal-Assisted Chemical Etching of Silicon. *Nano Lett.* **2011**, *11*, 2369–2374.
- 38. Hildreth, O. J.; Lin, W.; Wong, C. P. Effect of Catalyst Shape and Etchant Composition on Etching Direction in Metal-Assisted Chemical Etching of Silicon to Fabricate 3d Nanostructures. *ACS Nano* **2011**, *3*, 4033–4042.
- 39. Peng, K.; Lu, A.; Zhang, R.; Lee, S. Motility of Metal Nanoparticles in Silicon and Induced Anisotropic Silicon Etching. *Adv. Funct. Mater.* **2008**, *18*, 3026–3035.
- 40. Bashouti, M. Y.; Sardashti, K.; Schmitt, S. W.; Pietsch, M.; Ristein, J.; Haick, H.; Christiansen, S. H. Oxide-Free Hybrid Silicon Nanowires: From Fundamentals to Applied Nanotechnology. *Prog. Surf. Sci.* **2013**, *88*, 39–60.
- 41. Peng, K. Q.; Yan, Y.; Gao, S. P.; Zhu, J. Dendrite-Assisted Growth of Silicon Nanowires in Electroless Metal Deposition. *Adv. Funct. Mater.* **2012**, *13*, 127–132.
- 42. Chen, T.-G.; Huang, B.-Y.; Liu, H.-W.; Huang, Y.-Y.; Pan, H.-T.; Meng, H.-F.; Yu, P. Flexible Silver Nanowire Meshes for High-Efficiency Microtextured Organic-Silicon Hybrid Photovoltaics. *ACS Appl. Mater. Interfaces* **2012**, *4*, 6857–6864.